Journal of Controlled Release 174 (2014) 177–187

Contents lists available at ScienceDirect

Journal of Controlled Release

journal homepage: www.elsevier.com/locate/jconrel

PEGylation improves the receptor-mediated transfection efficiency of peptide-targeted, self-assembling, anionic nanocomplexes ☆

Aristides D. Tagalakis [a,*], Gavin D. Kenny [a], Alison S. Bienemann [b], David McCarthy [c], Mustafa M. Munye [a], Hannah Taylor [b], Marcella J. Wyatt [b], Mark F. Lythgoe [d], Edward A. White [b], Stephen L. Hart [a]

[a] Wolfson Centre for Gene Therapy of Childhood Disease, UCL Institute of Child Health, University College London, 30 Guilford Street, London WC1N 1EH, UK
[b] Functional Neurosurgery Research Group, School of Clinical Sciences, AMBI Labs, University of Bristol, Southmead Hospital, Bristol BS10 5NB, UK
[c] UCL School of Pharmacy, University College London, 29-39 Brunswick Square, London WC1N 1AX, UK
[d] UCL Centre for Advanced Biological Imaging, Division of Medicine and Institute of Child Health, University College London, 72 Huntley Street, London, WC1E 6DD, UK

ARTICLE INFO

Article history:
Received 6 October 2013
Accepted 13 November 2013
Available online 22 November 2013

Keywords:
Gene therapy
Targeted
Anionic
Nanoparticle
MRI
Self-assembling

ABSTRACT

Non-viral vector formulations comprise typically complexes of nucleic acids with cationic polymers or lipids. However, for *in vivo* applications cationic formulations suffer from problems of poor tissue penetration, non-specific binding to cells, interaction with serum proteins and cell adhesion molecules and can lead to inflammatory responses. Anionic formulations may provide a solution to these problems but they have not been developed to the same extent as cationic formulations due to difficulties of nucleic acid packaging and poor transfection efficiency. We have developed novel PEGylated, anionic nanocomplexes containing cationic targeting peptides that act as a bridge between PEGylated anionic liposomes and plasmid DNA. At optimized ratios, the components self-assemble into anionic nanocomplexes with a high packaging efficiency of plasmid DNA. Anionic PEGylated nanocomplexes were resistant to aggregation in serum and transfected cells with a far higher degree of receptor-targeted specificity than their homologous non-PEGylated anionic and cationic counterparts. Gadolinium-labeled, anionic nanoparticles, administered directly to the brain by convection-enhanced delivery displayed improved tissue penetration and dispersal as well as more widespread cellular transfection than cationic formulations. Anionic PEGylated nanocomplexes have widespread potential for *in vivo* gene therapy due to their targeted transfection efficiency and ability to penetrate tissues.

1. Introduction

There is great interest in developing nanocomplex formulations for gene delivery *in vivo* and for therapeutic applications as alternatives to viral vectors, due to their ability to package a wide range of nucleic acids, their low immunogenicity which allows repeated administration and their potential for chemical modification of vector components to optimize performance [1,2]. Non-viral vectors for gene or siRNA delivery usually comprise formulations of cationic polymers or liposomes that self-assemble electrostatically on mixing with nucleic acids at optimized ratios to form cationic nanocomplexes that are often very effective as *in vitro* transfection agents [3–6] but often display poor transfection efficiency *in vivo* due to their aggregation in serum and to non-specific, charge-mediated binding to anionic cell surfaces and extracellular adhesion molecules [7–9]. Stealth coatings, of nanocomplexes, for example by PEGylation, can enhance serum stability and minimize non-specific interactions but usually reduce transfection efficiencies [10,11].

An alternative approach is to formulate anionic nanocomplexes that offer the advantages of better targeting specificity, lower cytotoxicity and less interaction with serum components when compared to cationic formulations [12–14]. However, the use of anionic nanocomplexes has proven problematic due to the inherent problem of achieving self-assembly with anionic vector components and nucleic acids of the same charge [15]. Anionic nanocomplexes also display poor transfection efficiency due to charge repulsion at the anionic cell surface and consequently poor cell binding and uptake. Strategies developed to overcome these challenges include using cationic agents such as Ca^{2+} cations [14,16–19] or protamine [20–22] to act as an electrostatic bridge between anionic lipids and nucleic acids, the use of anionic reagents such as polyglutamate to coat cationic nanoparticles with an anionic shell [23,24] or by formulating nanoparticles with pH-tunable lipids [25]. These anionic formulations and strategies have all shown promise for *in vitro* and *in vivo* delivery of DNA and siRNA indicating their potential for non-viral genetic therapies.

We have previously described a cationic receptor-targeted nanocomplex (RTN), comprising a mixture of cationic liposomes (L), a sixteen lysine peptide with a cyclic seven amino acid targeting domain

* Corresponding author: Tel.: +44 2079052817; fax: +44 2079052810.
E-mail address: a.tagalakis@ucl.ac.uk (A.D. Tagalakis).

0168-3659/$ – see front matter © 2013 The Authors. Published by Elsevier B.V. All rights reserved.
http://dx.doi.org/10.1016/j.jconrel.2013.11.014

(P) and plasmid DNA (D) which have achieved efficient *in vivo* gene delivery in the airway epithelium [26,27], tumors [28–30] and vascular tissues [31,32]. Furthermore, we recently have described anionic nanocomplexes that comprised a peptide with a neurotensin receptor-targeting motif and an anionic liposome (1:1 formulation of DOPG: DOPE) which showed targeted transfection *in vitro* and displayed much better distribution in rat brain than homologous cationic nanocomplexes administered by CED [33]. In this anionic nanocomplex we proposed that the peptide provides a cationic bridge between anionic liposomes and nucleic acids while also providing targeting properties via the receptor-binding peptide ligand.

The peptide ligand YGLPHKF in peptide Y was identified by biopanning a phage peptide library and closely resembles part of a targeting protein expressed by the intracellular pathogen *Legionella pneumophila* [31,34] although the identity of the receptor is unknown [35]. However, we have demonstrated that this peptide mediates targeted delivery of siRNA in cationic nanocomplexes to cells of neuronal origin [34,36]. In this study we have adapted this formulation to create anionic nanocomplexes by substituting cationic liposomes with anionic liposomes and adjusting the ratio of peptide and liposome components appropriately. In particular we have explored *in vitro* the effects of PEGylation on the biophysical and transfection properties of the anionic RTNs. *In vivo*, we have compared anionic and cationic PEGylated RTNs for dispersal and transfection in rat brain administered by convection-enhanced delivery (CED), a method that can achieve widespread dispersion of therapeutics from a single administration [37–43].

2. Materials and methods

2.1. Materials

All lipids used in this study are shown in Supplementary Table 1. 1,2- dioleoyl-sn-glycero-3- phospho-(1′- rac-glycerol) (DOPG), 1,2-di-O-octadecenyl-3-trimethylammonium propane (DOTMA), 1,2-dioleoyl-sn-glycero-3-phosphoethanolamine (DOPE), 1,2-dioleoyl-*sn*-glycero-3-phosphoethanolamine-N-(lissamine rhodamine B sulfonyl) (DOPE-Rhodamine), 1,2-dipalmitoyl-*sn*-glycero-3-phosphoethanolamine-N-[methoxy(polyethylene glycol)-2000] (DPPE-PEG2000), 1,2-dioleoyl-*sn*-glycero-3-phosphoethanolamine-N-[methoxy(polyethylene glycol)-2000] (DOPE-PEG2000) and DOTMA/DOPE (1:1 molar ratio) were purchased from Avanti Polar Lipids (Alabaster, Alabama, USA). GdDOTA$(GAC_{12})_2$ was provided by Dr Botta (Alessandria, Italy) [44]. Peptide Y (K_{16}GACYGLPHKFCG; net charge +18), ligand YL (YGLPHKF; net charge +2) and ligand YSL (YKHPGFL; net charge +2) were synthesized by ChinaPeptides (Shanghai, China), while the non-targeting peptides PS (K_{16}GACH PPMSKLCG; net charge +18) and peptide K_{16} (KKKKKKKKKKKKKKKK; net charge +16) were synthesized by Alta Biosciences (Birmingham, UK). The plasmid pCI-Luc consists of the luciferase gene from pGL3 (Invitrogen, Paisley, UK) subcloned into pCI (Promega, Southampton, UK). The plasmid pEGFP-N1 (4.7 kb) containing the gene GFP was obtained from Clontech (Basingstoke, UK). The oligonucleotide primers and standards for qRT-PCR were provided by qStandard (Middlesex, UK) and were as follows: eGFP: forward primer 5′-CTTCAAGATCCGCC ACAACAT-3′ and reverse primer 5′-GGTGCTCAGGTAGTGGTTGTC-3′; Rpl13: forward primer 5′-CCCTACAGTTAGATACCACACCAA-3′ and reverse primer 5′-GATACCAGCCACCCTGAGC-3′; Beta actin: forward primer 5′-ACGGTCAGGTCATCACTATCG-3′ and reverse primer 5′-AGCC ACCAATCCACACAGA-3′; Sdha: forward primer 5′-TGGACCTTGTCGTC TTTGG-3′ and reverse primer 5′-TTTGCCTTAATCGGAGGAAC-3′.

2.2. Liposome formulation

Lipids were dissolved in chloroform at 10 mg/mL then a lipid film was produced in a rotary evaporator by slowly evaporating the chloroform. Lipids were rehydrated with sterile, distilled water while constantly rotated overnight, and then sonicated in a water bath to reduce their size. Anionic liposomes made were: DOPG:DOPE (L^A) at 1:1 molar ratio; DOPG:DOPE:DPPE-PEG2000 ($L^{AP}1$) at a molar ratio of 47.5:47.5:5 mol%, respectively; DOPG:DOPE:DOPE-PEG2000 ($L^{AP}2$) at a molar ratio of 47.5:47.5:5 mol%, respectively. An anionic liposome labeled with gadolinium and rhodamine (L^{APRG}) was prepared with a mixture of DOPG:DOPE:DOPE-PEG2000:DOPE-Rhodamine:GdDOTA $(GAC_{12})_2$ at a molar ratio of 39.5:39.5:5:1:15 mol%, respectively. A cationic liposome labeled with gadolinium and rhodamine (L^{CPRG}) was also formulated consisting of DOTMA:DOPE:DOPE-PEG2000: DOPE-Rhodamine:GdDOTA$(GAC_{12})_2$ at a molar ratio of 39.5:39.5: 5:1:15 mol%, respectively. A = anionic, P = PEGylated, C = cationic, R = rhodamine and G = gadolinium.

2.3. Nanoparticle formulation

Two methods of formulating anionic nanocomplexes were evaluated. In both, nanocomplexes were prepared in water at a range of molar charge ratios of L to D while the peptide P to D molar charge ratio was maintained constant at 3:1. Method 1 (L:D:P): DNA was first added to an anionic liposome (L^A, $L^{AP}1$ or $L^{AP}2$) and incubated for 15 min at room temperature and then the peptide was added with rapid mixing and incubated at room temperature for a further 20 min; Method 2 (P:D:L): the peptide was added to the DNA and incubated for 15 min at room temperature and then liposome was added with rapid mixing and incubated at room temperature for a further 20 min. Irrespective of the method of order of mixing, all molar charge ratios in this study refer to L:P:D. Cationic formulations LPD and L^{CPRG}PD were prepared in the order L:P:D as described previously; first, the peptide was added to the liposome DOTMA/DOPE or L^{CPRG} followed by addition of the DNA with rapid mixing and incubated for 30 min at room temperature to allow for complex formation [30]. The nanocomplexes prepared were termed LPD (liposome DOTMA/DOPE), L^ADP and PDL^A (liposome L^A), $PDL^{AP}1$ (liposome $L^{AP}1$), $PDL^{AP}2$ (liposome $L^{AP}2$), PDL^{APRG} (liposome L^{APRG}) and L^{CPRG}PD (liposome L^{CPRG}).

2.4. In vitro transfections

The murine neuroblastoma cell line Neuro-2A (ATCC, Teddington, UK), and the rat neuroblastoma cell lines B104 (ICLC, Genova, Italy) and B103 (AddexBio, San Diego, USA) were maintained in Dulbecco's Modified Eagle Medium, 1% non-essential amino acids, 1 mM sodium pyruvate and 10% FCS (Invitrogen, Paisley, UK). The human bronchial epithelial cells 16HBE14o− were provided by D. Gruenert (San Francisco, CA, USA) and were cultured in Eagle's Minimal Essential Medium with HEPES modification (Sigma-Aldrich, Poole, UK), 10% FCS and 2 mM L-glutamine. All cells were maintained at 37 °C in a humidified atmosphere in 5% carbon dioxide. Cells were seeded in 96-well plates at 2×10^4 per well 24 h prior to transfection. Following removal of growth medium, 200 μL of the complexes in OptiMEM containing 0.25 μg of plasmid DNA were added to the cells in replicates of six. Plates were centrifuged at 1500 rpm for 5 min (400 ×*g*) and incubated for 4 h at 37 °C, then the medium was replaced by the full growth medium and incubated for a further 24 h. Luciferase expression was then measured in cell extracts with a luciferase assay (Promega, Southampton, UK) in a FLUOstar Optima luminometer (BMG Labtech, Aylesbury, UK). The amount of protein present in each cell lysate was determined with the Bio-Rad protein assay reagent (Bio-Rad Laboratories, Hemel Hempstead, UK) in a FLUOstar Optima luminometer. Luciferase activity was expressed as relative light units per milligram of protein (RLU/mg). Each measurement was performed in groups of six and the mean determined.

Neuro-2A cells were seeded in 96-well plates at 1.2×10^4 per well 24 h prior to transfection with 175 μL complete serum-containing media. Twenty-four hours later, 25 μL of the complexes in OptiMEM

containing 0.25 μg of GFP plasmid DNA were added to the cells in replicates of six. Plates were centrifuged at 1500 rpm for 5 min (400 ×*g*) and incubated for 48 h at 37 °C. They were then firstly imaged (20× magnification) using an Olympus IX70 fluorescent microscope (Olympus, Southend-on-Sea, UK) then prepared for flow cytometry by detaching cells from the wells with 50 μL Trypsin-EDTA (Sigma-Aldrich, Poole, UK) and re-suspending them with 150 μL DPBS (Sigma-Aldrich, Poole, UK). Cells were then acquired with a BD FACSArray flow cytometer (BD Biosciences, Oxford, UK) and analyzed with FlowJo software v. 8.8.3 (Tree Star Inc., Ashland, Oregon, USA).

For competition experiments we modified a previously published method [45]. Neuro-2A cells were seeded in 96-well plates at 1.2×10^4 per well 24 h prior to transfection. The cells were pre-incubated with free ligands YL or YSL for 90 min prior to the addition of nanocomplexes at a final concentration of 100 μM. The media was then replaced with 200 μL of nanocomplexes per well containing 0.25 μg of GFP plasmid DNA that also contained free ligands YL or YSL at a final concentration of 100 μM. Plates were centrifuged at 1500 rpm for 5 min (400 ×*g*) and incubated for 4 h at 37 °C, then the medium was replaced by the full growth medium without any ligands and incubated for a further 48 h. They were then prepared for flow cytometry analysis as above.

2.5. Particle size and charge measurements

Nanocomplexes were prepared as above and diluted with distilled water to a final volume of 1 mL and a concentration of 5 μg/mL DNA. They were then analyzed for size and charge (ζ potential) using a Malvern Nano ZS (Malvern, UK). The data were then processed by software provided by the manufacturer, DTS version 5.03. All formulations had a polydispersity index (PDI) of less than 0.3.

2.6. Turbidity assay

The turbidity of nanocomplex suspension in different serum concentrations (0–50% v/v) was determined from absorbance at 500 nm on a FLUOstar Optima spectrophotometer with a corresponding amount of serum alone as a reference [46]. Nanocomplexes were formed as described above with 1 μg DNA in a volume of 200 μL, incubated at 37 °C and analyzed at regular time points over a 30 min period. Relative turbidity was determined by dividing the sample absorbance by the time zero value in water.

2.7. PicoGreen fluorescence quenching experiments

Briefly, 0.2 μg DNA was mixed with PicoGreen reagent (1:150) (Invitrogen, Paisley, UK) at room temperature in TE buffer and the DNA/PicoGreen mixture was then formulated into nanocomplexes with anionic liposome and cationic peptide as described above. Fluorescence was analyzed using a fluorescence plate reader, FLUOstar Optima (BMG Labtech, Aylesbury, UK).

In nanocomplex dissociation assays, heparin sulfate (Sigma-Aldrich, Poole, UK) was added to the PicoGreen-labeled nanocomplexes in a range of concentrations (0.05–2 U/mL). In each experiment, naked DNA stained with PicoGreen was used to normalize the PicoGreen signal detected from the nanocomplexes.

2.8. Transmission electron microscopy (TEM)

Prior to use, 300-mesh copper grid coated with a Formvar/carbon support film (Agar Scientific, Essex, UK) were "glow discharged" in an Emitech K350G system (Quorum Technologies, Essex, UK) for 15 s at 30 mA (positive polarity). The anionic nanocomplexes were prepared in water as described above then applied onto a grid and after 5 s dried by blotting with filter paper. The sample was then negatively stained with 1% uranyl acetate for 2–3 s, before blotting with filter paper and air-drying. Imaging was performed with a Philips CM120 BioTwin Transmission Electron Microscope and operated at an accelerating voltage of 120 kV. Images were captured using an AMT 5MP digital TEM camera (Deben UK Limited, Bury St. Edmunds, Suffolk, UK).

2.9. Cell proliferation assay

Cell viability was assessed in 96-well plates using the CellTiter 96 Aqueous One Solution Cell Proliferation Assay (Promega, Southampton, UK). Neuro-2A cells were seeded and transfected with anionic and cationic nanocomplexes as above, then, after 24 h, the media were substituted for growth media containing 20 μL of CellTiter 96 Aqueous One Solution reagent. Finally, after incubation for 2 h, absorbance at 490 nm was measured on a FLUOstar Optima spectrophotometer (BMG Labtech, Aylesbury, UK). Cell viability for each complex was expressed as a percentage of the viability of control cells.

2.10. In vivo CED procedures

All *in vivo* studies were performed in accordance with the University of Bristol animal care policies and with the authority of appropriate UK Home Office licenses. Adult male Wistar rats (Charles River, Margate, UK, 225 to 275 g) were anesthetized and placed in a small animal stereotaxic frame (Stoelting, Illinois, USA). All CED procedures were performed using a custom-made catheter with an outer diameter of 0.22 mm and inner diameter of 0.15 mm, composed of fused silica with a laser cut tip as described previously [43]. A total volume of 5 μL of anionic and cationic PEGylated nanoparticles incorporating Gadolinium and Rhodamine (190 ng eGFP/μL) for the striatum and 2.5 μL for the corpus callosum was delivered at an infusion rate of 2.5 μL/min. The Gadolinium dose delivered here is less than 4.5 μg, which is far less than the 50% lethal dose in rodents when the Gadolinium is chelated at 1–2 mg/kg or 100–200 mg/kg for the free ion [47]. Rats were culled 48 h following CED. For immunohistochemical analysis (IHC), animals were transcardially perfused with 4% paraformaldehyde. Brains were removed and placed in 4% paraformaldehyde for 24 h, then cryoprotected in 30% sucrose in order to be processed for histology. For qRT-PCR, brains were explanted and rapidly frozen at −80 °C until required.

2.11. MRI

MRI measurements were performed on a 9.4 T VNMRS horizontal bore scanner (Varian Inc. Palo Alto, CA) using a 59/26 Rapid quadrature volume coil. Fixed rat brains were imaged using a T_1-weighted gradient echo 3D sequence (TR = 17 ms, TE = 4 ms, FA = 52°, 40 μm isotropic resolution, Ave = 6). Distribution volumes were measured by segmenting the hyperintensities caused by the gadolinium containing nanoparticles using Amira (Visage Imaging Inc., San Diego, CA, USA).

2.12. Histological assessment and cell staining

Rat brains were cut into 35 μm thick coronal sections using a Leica CM1850 cryostat (Leica Microsystems, Wetzlar, Germany) at −20 °C. For fluorescent immunohistochemistry, fixed sections were mounted on gelatine-subbed slides. Once dry, the sections were washed with PBS for 5 min × 3. Sections were blocked in PBS plus 0.1% triton-x-100 containing 10% normal donkey serum (Sigma-Aldrich, Poole, UK) for 1 h at RT. They were then washed with 0.1% triton-x-100 in PBS for 5 min. Following washing, sections were incubated in the following primary antibodies: mouse anti-NeuN (1:300; Merck Millipore, MA, USA), rabbit anti-GFP (1:200; Merck Millipore, MA, USA). The next day, the primary antibody was removed and sections were washed with 0.1% triton-x-100 in PBS for 5 min × 3. Sections were incubated with donkey anti-Mouse Cy3 or donkey anti-rabbit Cy3 (1:300; Jackson Laboratories, Sacramento, CA, USA) and DAPI (1:200 of 1 mg/mL; Sigma-Aldrich, Poole, UK) at RT for 2 h in the dark and then washed with PBS for 5 min × 3. Sections were mounted in Fluorsave™

Reagent (Calbiochem®, Merck Millipore, Billerica, MA, USA) before viewing. Images were captured using the Stereo Investigator platform (MicroBrightField Bioscience, Williston, VT, USA) with a Leica DM5500 microscope (Leica Microsystems, Germany) and digital camera (Microbrightfield Bioscience, Williston, VT, USA). Some slides were visualized by confocal microscopy on a Carl Zeiss LSM710 laser scanning microscope system (Jena, Germany) at a magnification of ×400.

2.13. qRT-PCR

Rat brains (n = 3 per formulation) were collected in RNAlater (Invitrogen, Paisley, UK) and total RNA was extracted from rat brain using the RNeasy kit according to the manufacturer's instructions (Qiagen, Crawley, UK). RNA was checked for integrity using the Agilent 2100 Bioanalyzer (Wokingham, UK). All RNA samples had a RNA integrity number (RIN) of more than 9 indicating high quality RNA. Prior to reverse transcription, each sample underwent DNase treatment (Invitrogen, Paisley, UK) to eliminate any potential genomic DNA contamination. First-strand DNA was synthesized from 1 μg of DNase-treated RNA, using random hexamers and Superscript II reverse transcriptase (Invitrogen, Paisley, UK) in a 1 h reaction at 37 °C. eGFP, rat Succinate dehydrogenase complex subunit A (Sdha), rat Ribosomal protein L13 (Rpl13) and rat beta actin mRNA levels were then quantified by SYBR Green qRT-PCR using a an ABI PRISM 7000 Sequence Detection System (Applied Biosystems, Warrington, UK). The qRT-PCR assay conditions were: stage 1, 50 °C for 2 min; stage 2, 95 °C for 10 min; stage 3, 95 °C for 15 s, then 60 °C for 1 min and repeated 40 times. Amplification efficiency was 101% (eGFP), 102% (Rpl13), 102% (beta actin) and 103% (Sdha). Copy numbers for eGFP and the three housekeeping genes were derived from standard curves constructed of purified PCR products generated for each specific primer pair ranging from 10^7 to 10^1 copies for eGFP, Rpl13, beta actin and Sdha. Copy numbers of eGFP were normalized against the geometric mean of Rpl13 and beta actin, which were the most stable genes.

2.14. Statistical analysis

Data presented in this study are expressed as the mean ± standard deviation and were analyzed using a two-tailed, unpaired Student *t*-test or one-way ANOVA and Bonferroni post-hoc analysis where applicable. Probability values $p < 0.05$ were marked with *, $p < 0.01$ were marked with ** and $p < 0.001$ were marked with ***.

3. Results

3.1. Development and characterization of anionic nanoparticles

LDP (Method 1) or PDL (Method 2) nanocomplexes were formulated at anionic liposome:DNA (L:D) molar charge ratios from 5:1 to 1:1. Zeta potential analysis showed that LDP and PDL nanocomplexes became strongly anionic when the L:D molar charge ratio was 3.5:1 or greater with no significant size or charge differences (Fig. 1A and B).

PicoGreen fluorescence assays (Fig. 1S-A) showed that PDL formulations quenched fluorescence better than LDP formulations at the 5:3:1 molar charge ratio (37% quenching for LDP vs. 61% for PDL; $p < 0.01$) but there was no difference at the 4:3:1 ratio. Luciferase transfection efficiency comparisons in B104 and 16HBE14o− cells (Fig. 1S-B and C, respectively) showed that the PDL order of mixing was substantially better than LDP at all molar charge ratios. Therefore, based on packaging and transfection efficiencies, the PDL method of mixing was used thereafter for all anionic nanocomplexes.

Anionic liposomes (DOPG/DOPE) were then prepared with PEGylated lipids incorporated at 5% molar ratios and these liposomes were used to prepare the anionic PEGylated nanocomplexes $PDL^{AP}1$, containing the DPPE-PEG2000 liposome, and $PDL^{AP}2$ containing DOPE-PEG2000. The PEGylated nanocomplexes were both prepared at molar charge ratios of 5:3:1 and 4:3:1 and were confirmed to be anionic (Fig. 1C). $PDL^{AP}2$ nanocomplexes were bigger than both the non-PEGylated PDL^{A} and cationic LPD (Fig. 1C) while they were also less anionic (e.g. −36 mV for $PDL^{AP}2$ compared to −49 mV for PDL^{A}). The stability of nanocomplexes in 50% mouse serum was assessed where the turbidity of both PEGylated and non-PEGylated, anionic PDL nanocomplexes was less than half that of the cationic LPD formulation (Fig. 1D).

The ability of anionic nanocomplexes to package DNA efficiently and to dissociate following heparin challenge in order to release intact DNA was then assessed. PicoGreen-labeled DNA was formulated into cationic LPD and anionic PDL, PEGylated and non-PEGylated nanocomplexes at 4:3:1 molar charge ratios. Packaging was inferred from quenching of fluorescence compared to free DNA as 100%. Non-PEGylated PDL^{A} at 65% quenching, packaged less well than cationic LPD at 85% quenching, although PEGylation improved packaging in anionic formulations with both $PDL^{AP}1$ and $PDL^{AP}2$ also quenching DNA fluorescence by 80% (Fig. 2). On the other hand, PDL^{A} was the least sensitive formulation to heparin with fluorescence increasing only to 48.8%, even in the presence of 2 U/mL heparin, whereas cationic LPD only required 0.4 U/mL heparin to achieve 50% dissociation. PEGylation of anionic nanocomplexes greatly increased their sensitivity to heparin, achieving 50% dissociation at 0.14 U/mL heparin for $PDL^{AP}1$ and 0.32 U/mL of heparin for $PDL^{AP}2$ nanocomplexes (Fig. 2).

Anionic PDL nanoparticle formulations were further characterized by negative staining transmission electron microscopy (TEM) to determine shape and morphology. Most nanocomplexes were spheres but with some rods, while $PDL^{AP}2$ also showed some 'doughnut' structures (Fig. 3). The majority of the spherical particles for each formulation were in the range determined by particle size analysis with no obvious differences between formulations.

3.2. Enhanced targeted cell transfection efficiency and viability of anionic PDLs

Anionic PDL formulations were then compared with cationic formulations for cytotoxicity and targeted transfection efficiency in three neuroblastoma cell lines, mouse Neuro-2a and rat B103 and B104. In MTS toxicity assays of transfected Neuro-2A cells (Fig. 4A) all three anionic formulations were less toxic than cationic LPD ($p < 0.01$). In Neuro-2A cells (Fig. 4B), both PEGylated anionic nanocomplexes were more efficient transfection agents than the non-PEGylated PDL^{A} ($p < 0.001$) with $PDL^{AP}2$ showing optimal transfection efficiency and receptor specificity. The targeted transfection efficiency of anionic nanocomplexes with the targeting peptide, peptide Y, was 17.6-fold, 80.3-fold and 75-fold higher than those with K_{16} and 5-fold, 2.6-fold and 11.7-fold higher than those with peptide PS for PDL^{A}, $PDL^{AP}1$ and $PDL^{AP}2$, respectively, while cationic LPD formulations with peptide Y were enhanced only 1.8-fold compared to K_{16} and 1.3-fold compared to PS, highlighting the greater targeting specificity of the anionic formulations. The transfection efficiency of $PDL^{AP}2$ containing peptide Y was significantly better than $PDL^{AP}1$ ($p < 0.01$) and this was also the more stable formulation in the heparin dissociation studies.

The same trends were observed in B103 cells (Fig. 4C) and B104 cells (Fig. 4D) where the targeted transfection efficiency and specificity of anionic $PDL^{AP}2$ was again significantly better than that of cationic LPD ($p < 0.001$). $PDL^{AP}2$ with peptide Y was about two-fold better than the scrambled PS formulation ($p < 0.05$) although both anionic and cationic formulations were significantly improved over non-targeting K_{16} formulations. In B104 cells (Fig. 4D) the transfection efficiency of peptide Y-targeted $PDL^{AP}2$ formulation was more than thirty-fold better than that that of the scrambled PS and non-targeting K_{16} formulations and almost 2-fold better than the peptide Y-targeted cationic LPD formulation.

The transfection efficiencies of anionic PEGylated formulations were then compared with the plasmid expressing enhanced green fluorescent protein (GFP) in Neuro-2A cells. Flow cytometry analysis showed that, in the presence of 10% serum, peptide Y-targeted $PDL^{AP}2$ transfected

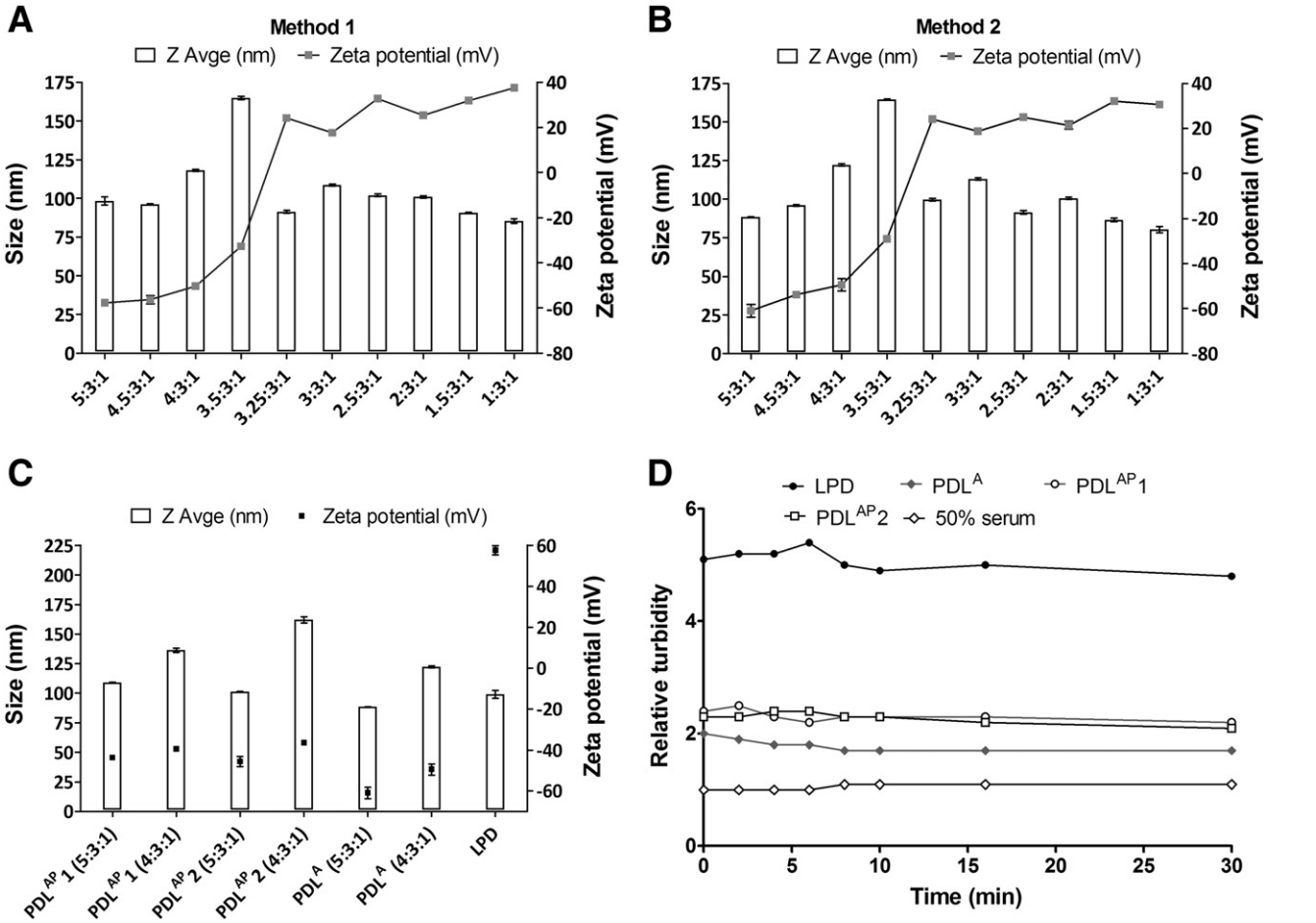

Fig. 1. Development of anionic nanoparticles and biophysical characterization. (A) Anionic L^{A}DP nanoparticles were prepared with Method 1 of mixing (L:D:P; liposome with DNA were mixed first followed by mixing with peptide Y) at different molar charge ratios and their size and charge was measured by dynamic light scattering. All formulations had a polydispersity index (PDI) of less than 0.2. (B) Anionic PDL^{A} nanoparticles were prepared with Method 2 of mixing (P:D:L; peptide Y with DNA were mixed first followed by mixing with the liposome) at different molar charge ratios and their size and charge was measured by dynamic light scattering. All formulations had a PDI of less than 0.2. (C) Anionic PEGylated PDL^{AP}1 and PDL^{AP}2 and non-PEGylated PDL^{A} nanoparticles made with Method 2 of mixing were prepared at different molar charge ratios and their size and charge was measured by dynamic light scattering and compared with that of cationic LPD. All formulations had a PDI of less than 0.3. (D) The effect of 50% serum concentration on the relative turbidity of cationic and anionic nanocomplexes over a 30 min incubation period. Cationic LPD nanocomplexes were made at a 1:4:1 weight ratio, whereas the anionic nanocomplexes (non-PEGylated PDL^{A} and PEGylated PDL^{AP}1 and PDL^{AP}2) were all made at a 4:3:1 molar charge ratio. Peptide Y was used for all formulations.

up to 65% of cells while Y-targeted cationic LPD formulations transfected a maximum of 22% cells ($p < 0.001$; Fig. 4E). In addition, targeted transfection specificity was again more evident with PDL^{AP}2 than LPD when comparing with K_{16} and PS-containing formulations (Fig. 4E). The specificity of gene delivery by peptide Y was further demonstrated in competition experiments using excess free ligand YL (i.e. only the targeting motif of peptide Y) or excess free scrambled ligand YSL (i.e. only a scrambled motif). GFP transfection following peptide Y-mediated gene delivery was 44-fold and 8-fold reduced ($p < 0.001$ for both) when the gene transfer was performed in the presence of free ligand YL for PDL^{AP}2 and LPD nanocomplexes, respectively, whereas no significant difference was observed in the presence of free ligand YSL (Fig. 4F). There was no effect of ligand YL or ligand YSL on peptide PS-mediated gene transfer. Reduction in reporter gene transfection was also observed when the competition experiments were performed for luciferase expression in the presence of YL ligand (approximately 12-fold and 4-fold for PDL^{AP}2 and LPD, respectively; $p < 0.001$ for both), whereas no effect was observed in the presence of YSL (Fig. 2S). Fluorescent microscopy images also provided evidence of the high transfection efficiency of PDL^{AP}2 anionic nanoparticles (Fig. 5).

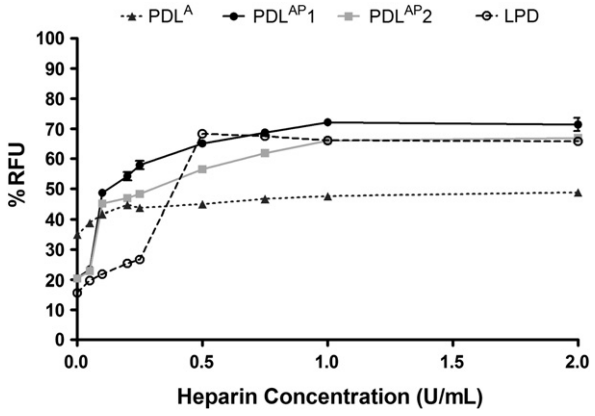

Fig. 2. Heparin dissociation studies to examine packaging properties of the nanocomplexes. The dissociation properties of anionic nanocomplexes PDL^{A}, PDL^{AP}1 and PDL^{AP}2 at 4:3:1 molar charge ratios and cationic nanocomplex LPD were investigated. PicoGreen fluorescence of complexes, after incubation with heparin (0–2 U/mL), was expressed as a percentage of RFU relative to free DNA. Peptide Y was used for all formulations.

3.3. In vivo administration by CED of anionic PDLs demonstrated significant brain distribution and transgene expression

Targeted, anionic and cationic, PEGylated formulations were prepared with liposomes labeled with fluorescent rhodamine and gadolinium, an MRI contrast agent (Table 1). Formulations containing GFP were administered to rat brains by CED into the corpus callosum and the

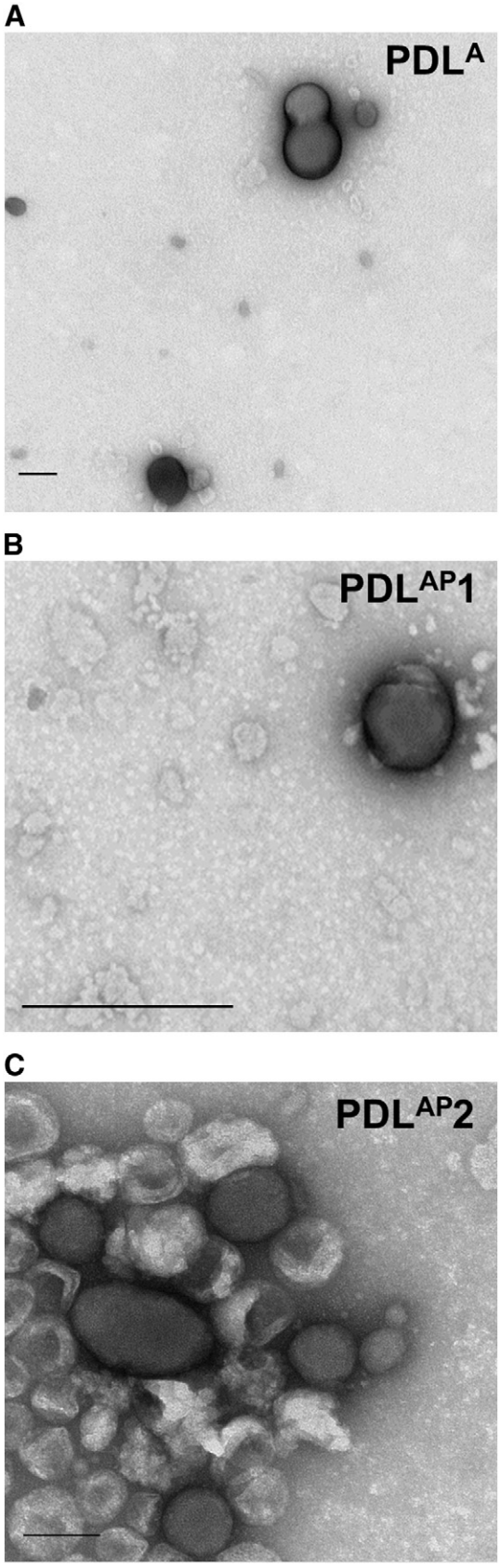

Fig. 3. Electron microscopy of nanocomplexes. Negative staining transmission electron microscopy was used to visualize (A) PDL^{A}, (B) $PDL^{AP}1$ and (C) $PDL^{AP}2$ nanoparticles. Scale bar = 100 nm for (A and C) and 500 nm for (B). Peptide Y was used for all formulations.

striatum then analyzed at 48 h for distribution by MRI. Analysis by MRI (Fig. 6A) and 3D reconstructions (Fig. 6B) showed that in the corpus callosum infusions the distribution volumes of anionic Ani PDL^{APRG} formulations was increased approximately 2-fold ($p < 0.05$) and 22-fold ($p < 0.001$) compared to the cationic formulations Cat PDL^{APRG} and Cat $L^{CPRG}PD$, respectively (Fig. 6C). Distribution volumes for all formulations were lower in the striatum than the corpus callosum due to the denser nature of the tissue but an increase in distribution of anionic Ani PDL^{APRG} nanocomplexes compared to Cat PDL^{APRG} (5-fold; $p > 0.05$) and Cat $L^{CPRG}PD$ formulations (25-fold; $p < 0.01$) was observed in the striatum infusions.

Histological analysis of brain sections (Figs. 6D and 3S) also suggested better distribution of the anionic rather than cationic nanoparticles but was not quantified. Rat brain sections (Fig. 6E) showed that the rhodamine-labeled nanoparticles expressed GFP within the striatum as well as the cortex, where transfection occurred due to nanoparticles refluxed up the catheter tract on withdrawal of the cannula. Confirmation of GFP transgene expression was achieved by quantitative real time polymerase chain reaction (qRT-PCR) using samples of total RNA (Fig. 6F) from two regions of the brain (corpus callosum and striatum). Highest expression levels were achieved by cationic formulation Cat $PDL^{AP}2$ especially in the striatum, followed by the anionic formulation Ani $PDL^{AP}2$, with no statistical differences among the groups.

4. Discussion

Many of the limitations of synthetic nanoparticle formulations *in vivo*, such as poor tissue specificity, toxicity and rapid clearance from the circulation, relate to their cationic surface charges. Stealth coatings such as PEGylation overcome some of these problems but often lead to reduced transfection efficiency [11]. For these reasons, neutral and anionic nanocomplex formulations have gained traction in the field in recent years although the level of research remains far below that of cationic formulations. One of the first such approaches involved a formulation of anionic liposomes and cationic protamine with DNA, targeted to tumor cells by folate [48] and various derivatives of this formulation have been developed in recent years [21,22,49–51]. Other effective approaches of preparing anionic nanocomplexes involve the use of electrostatic, anionic coating agents such as hyaluronan, polyglutamate and chondroitin sulfate applied to a cationic core nanoparticle [52–55]. Such approaches have enabled the production of highly anionic nanoparticles that display comparable levels of transfection to cationic formulations but with advantages of greater specificity and lower cytotoxicity. Anionic DNA-delivery formulations have shown promising evidence of improved efficacy, biodistribution and reduced toxicity compared to cationic formulations when administered systemically for targeting of tumors [23,48,53,56]. Anionic formulations have also been described for siRNA transfection with similarly promising results [16,17,24,57,58]. There is therefore a need for more research into the potential of anionic formulations to optimize their design, formulation and applications.

We are developing a platform of anionic, targeted nanocomplex formulations comprising a mixture of peptide ligands and anionic liposomes that self-assemble into anionic nanocomplexes with DNA at optimized ratios of components and order of mixing. Our first such formulation displayed far superior distribution in rat brain than homologous cationic nanocomplexes following CED administration [33]. Here we have focused on developing this formulation further, investigating the effects of PEGylation and an alternative targeting moiety, peptide Y. We relate the biophysical properties of these novel nanocomplexes to their transfection efficiencies *in vitro* and *in vivo* in rat brain, as well as brain distribution by MRI.

Anionic nanocomplex formulation protocols were first optimized in terms of method of mixing and molar charge ratios, then structural and functional studies were performed to compare the PEGylated formulations with non-PEGylated anionic and cationic formulations. The

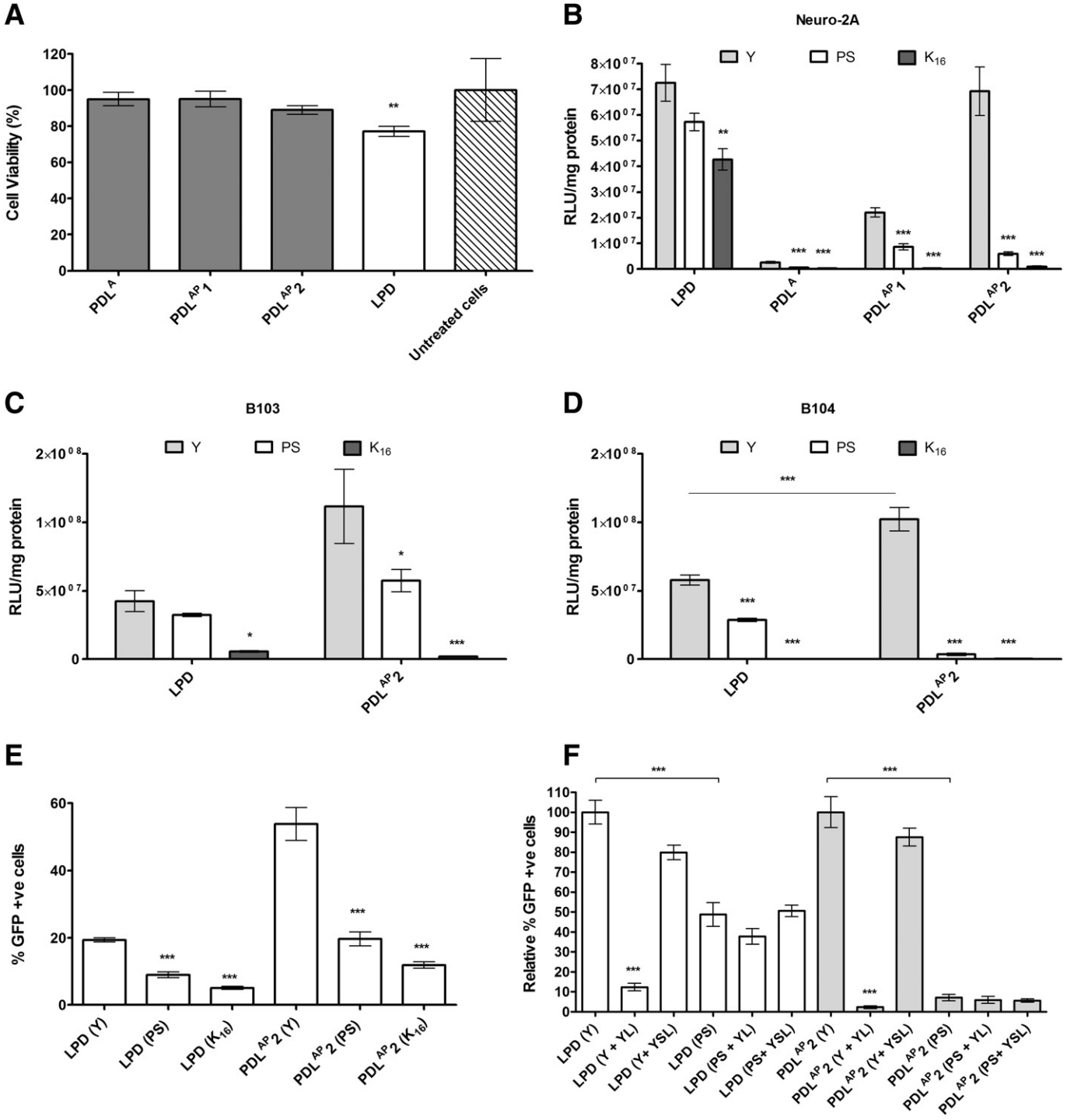

Fig. 4. *In vitro* transfections with anionic nanocomplexes show the targeting effect of peptide Y and lack of cytotoxicity. (A) Viability of Neuro-2A cells following transfection for 24 h with PDL^{A}, $PDL^{AP}1$, $PDL^{AP}2$ and LPD. Cationic nanocomplexes were made at a weight ratio of 1:4:1 (L:P:D) and the anionic nanocomplexes at a molar charge ratio of 4:3:1 (L:P:D). Viability values were normalized to the untransfected control cells. Anionic formulations are shown in gray and cationic formulations in white. Peptide Y was used for all formulations. (B) Nanocomplexes LPD, PDL^{A}, $PDL^{AP}1$ and $PDL^{AP}2$ were used in luciferase transfections in Neuro-2A cells, (C) LPD and $PDL^{AP}2$ in B103 cells and (D) LPD and $PDL^{AP}2$ in B104 cells. All were made with 3 different peptides: peptide Y, scrambled peptide PS and peptide K_{16}. Cationic nanocomplexes were made at 1:4:1 weight ratio, whereas all anionic were made at 4:3:1 molar charge ratio. (E) Cationic LPD nanocomplexes (weight ratio 1:4:1) and anionic $PDL^{AP}2$ nanocomplexes at 4:3:1 molar charge ratio and made with three different peptides (peptide Y, scrambled peptide PS and peptide K_{16}) were used in GFP transfections in Neuro-2A cells in serum-containing media. 48 h later the cells were trypsinized and analyzed by flow cytometry for GFP expression. (F) Cationic LPD nanocomplexes (weight ratio 1:4:1) and anionic $PDL^{AP}2$ nanocomplexes at 4:3:1 molar charge ratio made with two different peptides (peptide Y and scrambled peptide PS) were used in GFP transfections in Neuro-2A cells. Competitive inhibition of peptide Y-mediated gene delivery was performed either in the presence or in the absence of free ligand YL or free scrambled ligand YSL and serum. The cells were pre-incubated with the free ligands at a concentration of 100 μM for 90 min prior to the addition of nanocomplexes. The graph shows %GFP gene expression relative to LPD (Y) for the cationic nanoparticles and relative to $PDL^{AP}2$ (Y) for the anionic nanoparticles. Each column represents the mean ± SD from six wells. All transfections were performed in groups of six and mean values were calculated. Asterisks indicate comparisons of specific formulations with statistical significance (*, $p < 0.05$; **, $p < 0.01$; ***, $p < 0.001$).

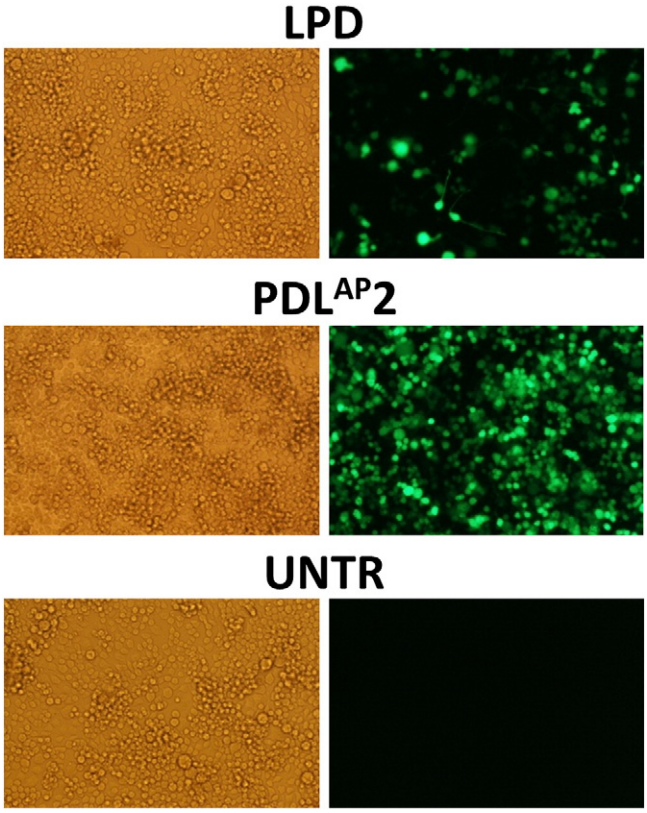

Fig. 5. GFP transfection efficiency of the PEGylated anionic nanoparticles is higher compared with a cationic counterpart. Two formulations, one cationic (LPD) and one anionic ($PDL^{AP}2$), were used to transfect Neuro-2A cells in serum-containing media. GFP expression was observed by epifluorescence microscopy 48 h later (representative cells are shown in phase-contrast and transfected cells appear green; 10× magnification). Peptide Y was used for all formulations. UNTR = untransfected cells.

cationic LPD nanoparticles had a similar size to the anionic non-PEGylated PDL^{A}. The anionic PEGylated nanoparticles were slightly larger in diameter than non-PEGylated anionic formulations, while their charge was less anionic due probably to PEG shielding. TEM images of anionic nanoparticles showed that there were no significant differences in morphology between the different PEGylated and non-PEGylated anionic formulations and cationic LPD formulations reported previously [34].

DNA packaging was significantly less efficient in anionic PDL^{A} formulations than in cationic LPD although PEGylation improved it to 80% from 65% in the non-PEGylated anionic formulation, which matched that of the cationic LPD formulation with approximately 85% efficiency. We then tested nanoparticle stability using mouse serum at 50% concentration (v/v) which approximates *in vivo* conditions [46]. PEGylated and non-PEGylated PDL^{A} formulations were far more stable in serum than cationic nanocomplexes which aggregated due to their interactions with anionic serum proteins [59]. Aggregation of cationic liposomes leads to reduced bioavailability, increased toxicity, reduced binding to cells and clearance *in vivo* of cationic nanoparticles by the reticuloendothelial system (RES) [46,60] and so we anticipate improved properties for anionic nanoparticles administered systemically.

While extracellular stability is an essential requirement for an efficient nucleic acid delivery formulation, effective transfection is also influenced by the ease of release of the cargo within the cell [36]. The cationic LPD formulation dissociated more easily and to a greater extent after treatment with heparin than PDL^{A}. However, PEGylation greatly enhanced the dissociation potential of anionic nanocomplexes particularly for $PDL^{AP}1$. The PEGylated lipid moiety in $PDL^{AP}1$ is a C16 saturated acyl chain while in $PDL^{AP}2$ it is a C18 unsaturated acyl chain. Longer acyl chains (C18 vs. C16) strengthen membrane cohesion of liposomes and this may explain the greater stability of $PDL^{AP}2$ [61]. In addition, PEG-lipids with the shortest acyl chain, provided the least liposome protection with rapid elimination of the liposomes from the circulation within 1 h after liposome injection [62]. The different sensitivities of PEGylated and non-PEGylated anionic nanocomplexes to heparin, may be explained by the greater anionic charge of the latter increasing resistance to dissociation. Toxicity assays showed that there was no difference between the PEGylated and non-PEGylated anionic formulations although there was some evidence of toxicity for the cationic formulations consistent with previous studies comparing anionic and cationic formulations [21,22,24].

We then compared the transfection efficiencies of the anionic formulations in different cell lines using different peptides, targeting (peptide Y) and non-targeting (peptides PS and K_{16}). Comparing peptide Y-targeted nanocomplexes, $PDL^{AP}2$ formulations produced significantly better luciferase transfection efficiencies than $PDL^{AP}1$ and similar to the efficiency of a cationic LPD formulation, while non-PEGylated PDL^{A} was far less efficient. GFP transfections also showed the greater transfection efficiency of $PDL^{AP}2$ when compared to $PDL^{AP}1$ and cationic LPD formulations.

Peptide Y-targeted anionic formulations produced much better transfection efficiencies than their non-targeted counterparts containing peptide PS or K_{16} in all cell lines examined, suggesting receptor-specific transfection. The receptor for peptide Y is unknown and so to evaluate receptor-mediated transfection specificity, cells were incubated with the competing peptide ligand, YL, before transfecting with peptide Y-containing nanocomplexes. This led to reduced transfection of both peptide Y-targeted anionic and cationic nanocomplexes, although the degree of inhibition of transfection was much greater with the anionic formulation. The scrambled control peptide, YSL, had no effect on transfection in targeted formulations, while transfections of cells containing non-targeting peptide PS were not affected by either YL or YSL. These studies support the hypothesis that anionic nanocomplexes transfect by receptor-specific pathways, while cationics transfect by charge-mediated non-specific routes, which can be enhanced by a targeting peptide ligand.

In relating differences in transfection efficiency to biophysical properties, PDL^{A}, the least effective transfection agent, possessed the highest anionic charge and was the least efficient formulation for both DNA packaging and release, although its high anionic charge was associated with significantly higher specificity for ligand-mediated transfection than that of cationic LPD. The high anionic surface charge would reduce cell surface interactions and endocytosis and this, combined with the poor DNA release kinetics help to explain the poor transfection

Table 1
Composition of liposomes and associated size and zeta potential of nanocomplexes as measured by dynamic light scattering. The molar ratio of each lipid that is used to make the 3 liposomes is shown in parentheses. Cat $L^{CPRG}PD$ was made at 1:4:1 weight ratio, Cat PDL^{APRG} was made at 3:3:1 molar charge ratio and Ani PDL^{APRG} was made at 4:3:1 molar charge ratio. Peptide Y was used for all formulations.

Liposome	Lipid 1 (mol %)	Lipid 2 (mol %)	Lipid 3 (mol %)	Lipid 4 (mol %)	Lipid 5 (mol %)	LPD/PDL	Size (nm)	ζ potential (mV)
L^{CPRG}	DOTMA (39.5)	DOPE (39.5)	DOPE-PEG2000 (5)	GdDOTA $(GAC_{12})_2$ (15)	DOPE-Rhodamine (1)	Cat $L^{CPRG}PD$	186.0 (± 0.1)	+57.0 (±0.8)
L^{APRG}	DOPG (39.5)	DOPE (39.5)	DOPE-PEG2000 (5)	GdDOTA $(GAC_{12})_2$ (15)	DOPE-Rhodamine (1)	Cat PDL^{APRG}	149.8 (±2.1)	+16.9 (±0.1)
L^{APRG}	DOPG (39.5)	DOPE (39.5)	DOPE-PEG2000 (5)	GdDOTA $(GAC_{12})_2$ (15)	DOPE-Rhodamine (1)	Ani PDL^{APRG}	160.5 (±2.7)	−37.9 (±5.3)

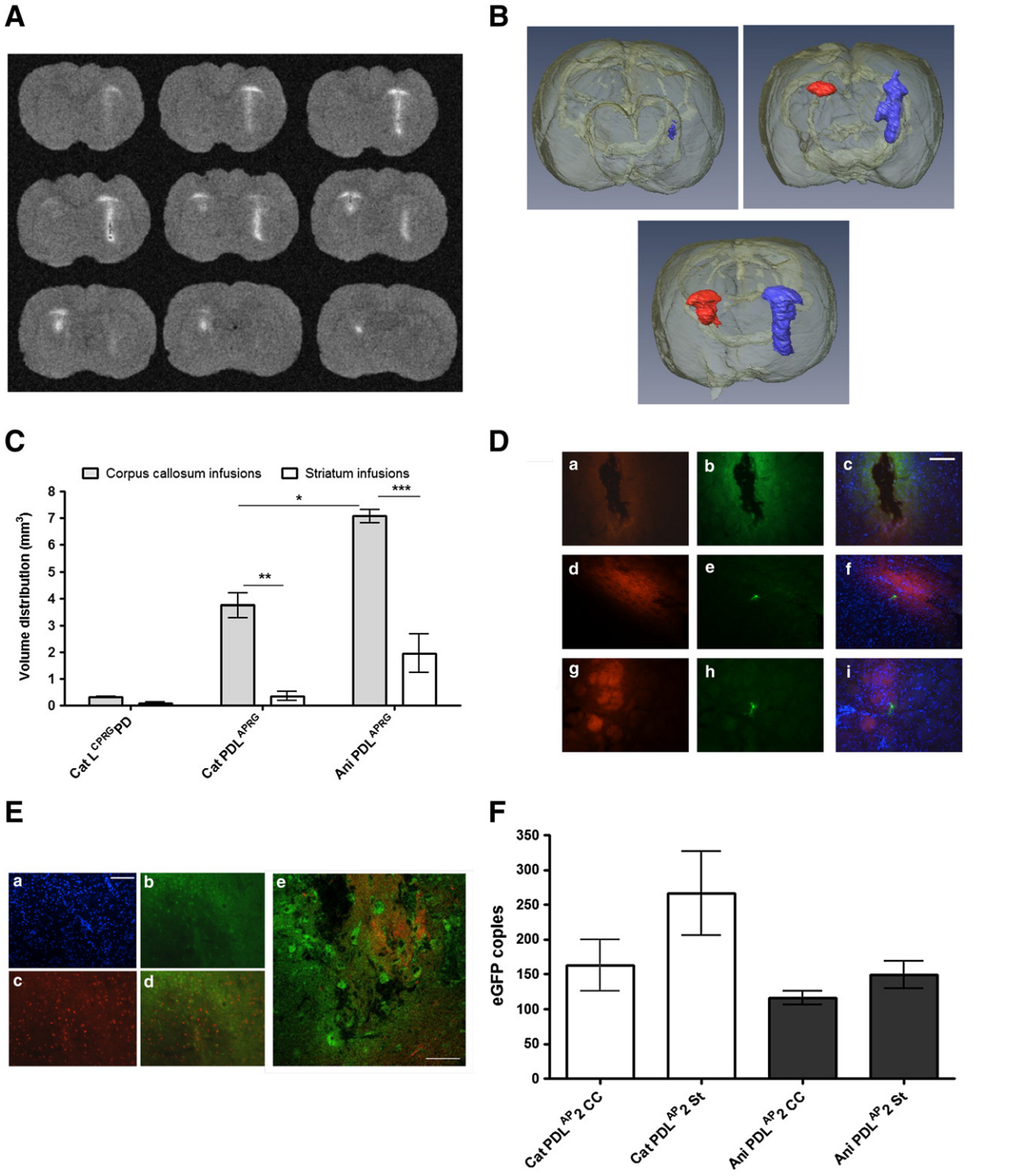

Fig. 6. *In vivo* distribution assessment of charged PEGylated nanoparticles into the striatum and corpus callosum after CED by MRI and histology and reporter gene delivery assessment by qRT-PCR. (A) Optimized 3D T_1-weighted gradient echo scans were performed to allow visualization of the gadolinium in the nanoparticles (representative scans from a rat that received Ani PDL^{APRG} nanoparticles), and these data (B) were reconstructed as 3D datasets to allow volumetric distribution analyses after CED in the striatum (red) and corpus callosum (blue) between cationic PEGylated nanoparticles Cat L^{CPRG}PD (left; 1:4:1 weight ratio) and Cat PDL^{APRG} (right; 3:3:1 molar charge ratio) and anionic PEGylated nanoparticles Ani PDL^{APRG} (bottom; 4:3:1 molar charge ratio). (C) Distribution of the anionic and cationic PEGylated nanoparticles following infusions in the striatum and corpus callosum at 48 h post administration was measured. Values are the means of 3 animals ± standard deviation (*, $p < 0.05$; **, $p < 0.01$; ***, $p < 0.001$). (D) Histological assessment in the striatum of (a–c) cationic PEGylated Cat L^{CPRG}PD nanoparticles, (d–f) Cat PDL^{APRG} nanoparticles, (g–i) anionic Ani PDL^{APRG} nanoparticles. (a, d, g) refer to rhodamine spread, (b, e, h) to GFP expression, (c, f,i) to the corresponding merged images which show the cellular nature of the striatum by DAPI staining. (E) Cat PDL^{APRG} nanoparticles have shown clear distribution, with several neuronal specific cells detected in the striatum. (a) DAPI stained cells, (b) GFP transfection, (c) NeuN antibody staining and (d) merged panel b and c. Scale bar = 100 μm; (e) confocal image from the cortex, whereby reflux has allowed visualization of several GFP positive cells following administration of Ani PDL^{APRG} nanoparticles. Scale bar = 20 μm. (F) Functional delivery of the eGFP plasmid by the cationic (Cat PDL^{AP}2 at 3:3:1 molar charge ratio) and anionic (Ani PDL^{AP}2 at 4:3:1 molar charge ratio) PEGylated nanoparticles was also assessed by qRT-PCR. These two formulations were made without imaging markers. Values represent the mean of the mRNA copies of 3 animals per group ± standard deviation. Peptide Y was used for all formulations. CC = corpus callosum, St = striatum.

efficiency compared to the cationic LPD. The improved transfection efficiency of PEGylated anionic formulations was associated with improved dynamic properties of the nanocomplexes in that they both packaged and released DNA more effectively than the non-PEGylated formulation and had lower anionic surface charge. In fact the optimal PEGylated formulation PDL^{AP}2 was a better transfection agent than even the cationic LPD, displaying a much higher degree of receptor-mediated transfection than cationic formulations. Of the two PEGylated formulations PDL^{AP}2 was slightly more stable to heparin-mediated dissociation than PDL^{AP}1 but otherwise presented with similar biophysical properties of size, charge and morphology. Thus PDL^{AP}2 may better retain its structural integrity during the transfection process in the anionic environment of the cell surface while retaining greater dynamic properties for DNA release within the cell, and hence achieve the greater transfection efficiencies observed.

We then investigated an *in vivo* application involving direct injection of nanoparticles to the brain by CED where anionic formulations offer the promise, of more widespread dispersal of nanoparticles from a single administration as they are less likely to adhere to cells non-specifically than similarly sized cationic nanoparticles [33,43], while other studies suggested that surface modification by PEGylation further enhanced distribution of anionic [63] but not of cationic nanoparticles [56,63]. In this study, nanocomplex formulations were labeled with gadolinium and rhodamine to enable detection by MRI and fluorescence microscopy, respectively [33]. Formulations compared for dispersal within the brain and transfection included, i) an anionic PDL^{AP}2-based formulation, Ani PDL^{APRG}, ii) a cationic formulation, Cat PDL^{APRG}, containing the same anionic liposome as PDL^{AP}2 but formulated with a lower amount of the anionic liposome (DOPG/DOPE) to make cationic nanocomplexes, and iii) a second cationic nanocomplex, Cat L^{CPRG}PD, prepared with cationic liposomes. The distribution of the anionic formulation by MRI was greater than either cationic formulation in both striatum and corpus callosum. The difference in distribution between the Cat L^{CPRG}PD and Cat PDL^{APRG}, may be attributed to the higher positive charge (+57.0 and +16.9 mV, respectively) (Table 1) leading to an increase in non-specific binding close to the cannula tip [63]. Distribution for all formulations was greater in the corpus callosum infusions due to the more compact nature of the striatum and the consequent importance of size limitations on distribution. The qRT-PCR analysis confirmed that GFP transgene expression was achieved in two regions of the brain (corpus callosum and striatum). All formulations achieved transgene expression in both brain areas with no statistical differences among the different groups. The higher local concentration of the cationic formulation may provide an advantage for transfection near the injection site compared to the anionic formulations, which are better dispersed but more diluted, reducing their local transfection efficiency. Future studies will be required to investigate optimal dosage for anionic formulations. The potential for efficient, targeted gene expression from anionic nanocomplexes combined with their improved distribution by CED suggests their utility for delivery of therapeutic genes to the brain.

5. Conclusions

In this study we describe a novel, multifunctional, anionic nanocomplex and demonstrated that optimized PEGylation strategies enhanced transfection efficiency and receptor-targeted specificity, possibly by lowering repulsion forces from the anionic moieties on the cell surfaces. This contrasts with cationic synthetic nanocomplex formulations where PEGylation typically reduces transfection efficiency. Distribution of gadolinium-labeled nanocomplex formulations in brain, administered by direct delivery, was improved in anionic formulations with levels of transfection equivalent to cationic formulations, demonstrating the potential for theranostic delivery of genes and contrast agents to allow monitoring of biodistribution by MRI.

Supplementary data to this article can be found online at http://dx.doi.org/10.1016/j.jconrel.2013.11.014.

Acknowledgments

This work was funded by the Engineering and Physical Sciences Research Council (EPSRC; EP/G061521/1) and by the Association for International Cancer Research (AICR). We would like to thank Dr Mauro Botta from the Università del Piemonte Orientale "Amedeo Avogadro" for providing the gadolinium-labeled lipid.

References

[1] D.J. Glover, H.J. Lipps, D.A. Jans, Towards safe, non-viral therapeutic gene expression in humans, Nat. Rev. Genet. 6 (2005) 299–310.
[2] G.D. Schmidt-Wolf, I.G. Schmidt-Wolf, Non-viral and hybrid vectors in human gene therapy: an update, Trends Mol. Med. 9 (2003) 67–72.
[3] H.M. Aliabadi, B. Landry, C. Sun, T. Tang, H. Uludag, Supramolecular assemblies in functional siRNA delivery: where do we stand? Biomaterials 33 (2012) 2546–2569.
[4] M. Elsabahy, A. Nazarali, M. Foldvari, Non-viral nucleic acid delivery: key challenges and future directions, Curr. Drug Deliv. 8 (2011) 235–244.
[5] D. Pezzoli, R. Chiesa, L. De Nardo, G. Candiani, We still have a long way to go to effectively deliver genes! J. Appl. Biomater. Funct. Mater. 10 (2012) 82–91.
[6] C. Scholz, E. Wagner, Therapeutic plasmid DNA versus siRNA delivery: common and different tasks for synthetic carriers, J. Control. Release 161 (2012) 554–565.
[7] R.I. Mahato, A. Rolland, E. Tomlinson, Cationic lipid-based gene delivery systems: pharmaceutical perspectives, Pharm. Res. 14 (1997) 853–859.
[8] M.A. Mintzer, E.E. Simanek, Nonviral vectors for gene delivery, Chem. Rev. 109 (2009) 259–302.
[9] W. Wang, W. Li, N. Ma, G. Steinhoff, Non-viral gene delivery methods, Curr. Pharm. Biotechnol. 14 (2013) 46–60.
[10] F.W. Huang, H.Y. Wang, C. Li, H.F. Wang, Y.X. Sun, J. Feng, X.Z. Zhang, R.X. Zhuo, PEGylated PEI-based biodegradable polymers as non-viral gene vectors, Acta Biomater. 6 (2010) 4285–4295.
[11] S. Mishra, P. Webster, M.E. Davis, PEGylation significantly affects cellular uptake and intracellular trafficking of non-viral gene delivery particles, Eur. J. Cell Biol. 83 (2004) 97–111.
[12] D.A. Balazs, W. Godbey, Liposomes for use in gene delivery, J. Drug Deliv. 2011 (2011) 326497.
[13] N.S. Chiaramoni, J. Gasparri, L. Speroni, M.C. Taira, V. Alonso Sdel, Biodistribution of liposome/DNA systems after subcutaneous and intraperitoneal inoculation, J. Liposome Res. 20 (2010) 191–201.
[14] S.D. Patil, D.G. Rhodes, D.J. Burgess, Biophysical characterization of anionic lipoplexes, Biochim. Biophys. Acta 1711 (2005) 1–11.
[15] C. Foged, H.M. Nielsen, S. Frokjaer, Liposomes for phospholipase A2 triggered siRNA release: preparation and *in vitro* test, Int. J. Pharm. 331 (2007) 160–166.
[16] M. Kapoor, D.J. Burgess, Physicochemical characterization of anionic lipid-based ternary siRNA complexes, Biochim. Biophys. Acta 1818 (2012) 1603–1612.
[17] J. Li, Y. Yang, L. Huang, Calcium phosphate nanoparticles with an asymmetric lipid bilayer coating for siRNA delivery to the tumor, J. Control. Release 158 (2012) 108–114.
[18] S.D. Patil, D.G. Rhodes, D.J. Burgess, Anionic liposomal delivery system for DNA transfection, AAPS J. 6 (2004) 13–22.
[19] C. Srinivasan, D.J. Burgess, Optimization and characterization of anionic lipoplexes for gene delivery, J. Control. Release 136 (2009) 62–70.
[20] Y. Chen, S.R. Bathula, J. Li, L. Huang, Multifunctional nanoparticles delivering small interfering RNA and doxorubicin overcome drug resistance in cancer, J. Biol. Chem. 285 (2010) 22639–22650.
[21] P. Sun, M. Zhong, X. Shi, Z. Li, Anionic LPD complexes for gene delivery to macrophage: preparation, characterization and transfection *in vitro*, J. Drug Target. 16 (2008) 668–678.
[22] H. Yuan, W. Zhang, Y.Z. Du, F.Q. Hu, Ternary nanoparticles of anionic lipid nanoparticles/protamine/DNA for gene delivery, Int. J. Pharm. 392 (2010) 224–231.
[23] T.J. Harris, J.J. Green, P.W. Fung, R. Langer, D.G. Anderson, S.N. Bhatia, Tissue-specific gene delivery via nanoparticle coating, Biomaterials 31 (2010) 998–1006.
[24] A. Schlegel, P. Bigey, H. Dhotel, D. Scherman, V. Escriou, Reduced *in vitro* and *in vivo* toxicity of siRNA-lipoplexes with addition of polyglutamate, J. Control. Release 165 (2013) 1–8.
[25] N. Mignet, C. Richard, J. Seguin, C. Largeau, M. Bessodes, D. Scherman, Anionic pH-sensitive PEGylated lipoplexes to deliver DNA to tumors, Int. J. Pharm. 361 (2008) 194–201.
[26] M.D. Manunta, R.J. McAnulty, A.D. Tagalakis, S.E. Bottoms, F. Campbell, H.C. Hailes, A.B. Tabor, G.J. Laurent, C. O'Callaghan, S.L. Hart, Nebulisation of receptor-targeted nanocomplexes for gene delivery to the airway epithelium, PLoS One 6 (2011) e26768.
[27] A.D. Tagalakis, R.J. McAnulty, J. Devaney, S.E. Bottoms, J.B. Wong, M. Elbs, M.J. Writer, H.C. Hailes, A.B. Tabor, C. O'Callaghan, A. Jaffe, S.L. Hart, A receptor-targeted nanocomplex vector system optimized for respiratory gene transfer, Mol. Ther. 16 (2008) 907–915.
[28] S.M. Grosse, A.D. Tagalakis, M.F. Mustapa, M. Elbs, Q.H. Meng, A. Mohammadi, A.B. Tabor, H.C. Hailes, S.L. Hart, Tumor-specific gene transfer with receptor-mediated

nanocomplexes modified by polyethylene glycol shielding and endosomally cleavable lipid and peptide linkers, FASEB J. 24 (2010) 2301–2313.
[29] G.D. Kenny, C. Villegas-Llerena, A.D. Tagalakis, F. Campbell, K. Welser, M. Botta, A.B. Tabor, H.C. Hailes, M.F. Lythgoe, S.L. Hart, Multifunctional receptor-targeted nanocomplexes for magnetic resonance imaging and transfection of tumours, Biomaterials 33 (2012) 7241–7250.
[30] A.D. Tagalakis, S.M. Grosse, Q.H. Meng, M.F. Mustapa, A. Kwok, S.E. Salehi, A.B. Tabor, H.C. Hailes, S.L. Hart, Integrin-targeted nanocomplexes for tumour specific delivery and therapy by systemic administration, Biomaterials 32 (2011) 1370–1376.
[31] S.A. Irvine, Q.H. Meng, F. Afzal, J. Ho, J.B. Wong, H.C. Hailes, A.B. Tabor, J.R. McEwan, S.L. Hart, Receptor-targeted nanocomplexes optimized for gene transfer to primary vascular cells and explant cultures of rabbit aorta, Mol. Ther. 16 (2008) 508–515.
[32] Q.H. Meng, S. Irvine, A.D. Tagalakis, R.J. McAnulty, J.R. McEwan, S.L. Hart, Inhibition of neointimal hyperplasia in a rabbit vein graft model following non-viral transfection with human iNOS cDNA, Gene Ther. 20 (2013) 979–986.
[33] G.D. Kenny, A.S. Bienemann, A.D. Tagalakis, J.A. Pugh, K. Welser, F. Campbell, A.B. Tabor, H.C. Hailes, S.S. Gill, M.F. Lythgoe, C.W. McLeod, E.A. White, S.L. Hart, Multifunctional receptor-targeted nanocomplexes for the delivery of therapeutic nucleic acids to the brain, Biomaterials 34 (2013) 9190–9200.
[34] A.D. Tagalakis, L. He, L. Saraiva, K.T. Gustafsson, S.L. Hart, Receptor-targeted liposome-peptide nanocomplexes for siRNA delivery, Biomaterials 32 (2011) 6302–6315.
[35] M.J. Writer, B. Marshall, M.A. Pilkington-Miksa, S.E. Barker, M. Jacobsen, A. Kritz, P.C. Bell, D.H. Lester, A.B. Tabor, H.C. Hailes, N. Klein, S.L. Hart, Targeted gene delivery to human airway epithelial cells with synthetic vectors incorporating novel targeting peptides selected by phage display, J. Drug Target. 12 (2004) 185–193.
[36] A.D. Tagalakis, L. Saraiva, D. McCarthy, K.T. Gustafsson, S.L. Hart, Comparison of nanocomplexes with branched and linear peptides for siRNA delivery, Biomacromolecules 14 (2013) 761–770.
[37] R.H. Bobo, D.W. Laske, A. Akbasak, P.F. Morrison, R.L. Dedrick, E.H. Oldfield, Convection-enhanced delivery of macromolecules in the brain, Proc. Natl. Acad. Sci. U. S. A. 91 (1994) 2076–2080.
[38] B.S. Carson Sr., Q. Wu, B. Tyler, L. Sukay, R. Raychaudhuri, F. DiMeco, R.E. Clatterbuck, A. Olivi, M. Guarnieri, New approach to tumor therapy for inoperable areas of the brain: chronic intraparenchymal drug delivery, J. Neurooncol. 60 (2002) 151–158.
[39] S.S. Gill, N.K. Patel, G.R. Hotton, K. O'Sullivan, R. McCarter, M. Bunnage, D.J. Brooks, C.N. Svendsen, P. Heywood, Direct brain infusion of glial cell line-derived neurotrophic factor in Parkinson disease, Nat. Med. 9 (2003) 589–595.
[40] D.R. Groothuis, S. Ward, A.C. Itskovich, C. Dobrescu, C.V. Allen, C. Dills, R.M. Levy, Comparison of 14C-sucrose delivery to the brain by intravenous, intraventricular, and convection-enhanced intracerebral infusion, J. Neurosurg. 90 (1999) 321–331.
[41] Y. Mardor, Y. Roth, Z. Lidar, T. Jonas, R. Pfeffer, S.E. Maier, M. Faibel, D. Nass, M. Hadani, A. Orenstein, J.S. Cohen, Z. Ram, Monitoring response to convection-enhanced taxol delivery in brain tumor patients using diffusion-weighted magnetic resonance imaging, Cancer Res. 61 (2001) 4971–4973.
[42] J. Voges, R. Reszka, A. Gossmann, C. Dittmar, R. Richter, G. Garlip, L. Kracht, H.H. Coenen, V. Sturm, K. Wienhard, W.D. Heiss, A.H. Jacobs, Imaging-guided convection-enhanced delivery and gene therapy of glioblastoma, Ann. Neurol. 54 (2003) 479–487.
[43] E. White, A. Bienemann, M. Sena-Esteves, H. Taylor, C. Bunnun, E. Castrique, S. Gill, Evaluation and optimization of the administration of recombinant adeno-associated viral vectors (serotypes 2/1, 2/2, 2/rh8, 2/9, and 2/rh10) by convection-enhanced delivery to the striatum, Hum. Gene Ther. 22 (2011) 237–251.
[44] F. Kielar, L. Tei, E. Terreno, M. Botta, Large relaxivity enhancement of paramagnetic lipid nanoparticles by restricting the local motions of the Gd(III) chelates, J. Am. Chem. Soc. 132 (2010) 7836–7837.
[45] P.J. Jost, R.P. Harbottle, A. Knight, A.D. Miller, C. Coutelle, H. Schneider, A novel peptide, THALWHT, for the targeting of human airway epithelia, FEBS Lett. 489 (2001) 263–269.
[46] Y. Zhang, T.J. Anchordoquy, The role of lipid charge density in the serum stability of cationic lipid/DNA complexes, Biochim. Biophys. Acta 1663 (2004) 143–157.
[47] J.G. Penfield, R.F. Reilly Jr., What nephrologists need to know about gadolinium, Nat. Clin. Pract. Nephrol. 3 (2007) 654–668.
[48] R.J. Lee, L. Huang, Folate-targeted, anionic liposome-entrapped polylysine-condensed DNA for tumor cell-specific gene transfer, J. Biol. Chem. 271 (1996) 8481–8487.
[49] G.L. Lorenzi, K.D. Lee, Enhanced plasmid DNA delivery using anionic LPDII by listeriolysin O incorporation, J. Gene Med. 7 (2005) 1077–1085.
[50] X. Sun, Z. Zhang, Optimizing the novel formulation of liposome-polycation-DNA complexes (LPD) by central composite design, Arch. Pharm. Res. 27 (2004) 797–805.
[51] J. Ye, A. Wang, C. Liu, Z. Chen, N. Zhang, Anionic solid lipid nanoparticles supported on protamine/DNA complexes, Nanotechnology 19 (2008) 285708.
[52] J.J. Green, E. Chiu, E.S. Leshchiner, J. Shi, R. Langer, D.G. Anderson, Electrostatic ligand coatings of nanoparticles enable ligand-specific gene delivery to human primary cells, Nano Lett. 7 (2007) 874–879.
[53] Y. He, G. Cheng, L. Xie, Y. Nie, B. He, Z. Gu, Polyethyleneimine/DNA polyplexes with reduction-sensitive hyaluronic acid derivatives shielding for targeted gene delivery, Biomaterials 34 (2013) 1235–1245.
[54] Z.X. Liao, S.F. Peng, Y.C. Ho, F.L. Mi, B. Maiti, H.W. Sung, Mechanistic study of transfection of chitosan/DNA complexes coated by anionic poly(gamma-glutamic acid), Biomaterials 33 (2012) 3306–3315.
[55] H. Tian, L. Lin, J. Chen, X. Chen, T.G. Park, A. Maruyama, RGD targeting hyaluronic acid coating system for PEI-PBLG polycation gene carriers, J. Control. Release 155 (2011) 47–53.
[56] J.A. MacKay, W. Li, Z. Huang, E.E. Dy, G. Huynh, T. Tihan, R. Collins, D.F. Deen, F.C. Szoka Jr., HIV TAT peptide modifies the distribution of DNA nanolipoparticles following convection-enhanced delivery, Mol. Ther. 16 (2008) 893–900.
[57] M. Kapoor, D.J. Burgess, Cellular uptake mechanisms of novel anionic siRNA lipoplexes, Pharm. Res. 30 (2013) 1161–1175.
[58] C. Lavigne, K. Slater, N. Gajanayaka, C. Duguay, E. Arnau Peyrotte, G. Fortier, M. Simard, A.J. Kell, M.L. Barnes, A.R. Thierry, Influence of lipoplex surface charge on siRNA delivery: application to the *in vitro* downregulation of CXCR4 HIV-1 co-receptor, Expert. Opin. Biol. Ther. 13 (2013) 973–985.
[59] J.P. Yang, L. Huang, Overcoming the inhibitory effect of serum on lipofection by increasing the charge ratio of cationic liposome to DNA, Gene Ther. 4 (1997) 950–960.
[60] P.R. Cullis, A. Chonn, S.C. Semple, Interactions of liposomes and lipid-based carrier systems with blood proteins: relation to clearance behaviour *in vivo*, Adv. Drug Deliv. Rev. 32 (1998) 3–17.
[61] M.A. Bellavance, M.B. Poirier, D. Fortin, Uptake and intracellular release kinetics of liposome formulations in glioma cells, Int. J. Pharm. 395 (2010) 251–259.
[62] W.M. Li, L.D. Mayer, M.B. Bally, Prevention of antibody-mediated elimination of ligand-targeted liposomes by using poly(ethylene glycol)-modified lipids, J. Pharmacol. Exp. Ther. 300 (2002) 976–983.
[63] J.A. MacKay, D.F. Deen, F.C. Szoka Jr., Distribution in brain of liposomes after convection enhanced delivery; modulation by particle charge, particle diameter, and presence of steric coating, Brain Res. 1035 (2005) 139–153.